INSTITUTE OF PHYSICS PUBLISHING INVERSE PROBLEMS

Inverse Problems **20** (2004) 1099–1116 PII: S0266-5611(04)71929-2

Efficient computation of lead field bases and influence matrix for the FEM-based EEG and MEG inverse problem

C H Wolters[1,2,3], **L Grasedyck**[2] **and W Hackbusch**[2]

[1] Scientific Computing and Imaging Institute, University of Utah, 50 S Central Campus Dr., Salt Lake City, UT 84112, USA
[2] Max Planck Institute for Mathematics in the Sciences, Inselstr. 22-26, 04103 Leipzig, Germany
[3] Max Planck Institute for Human Cognitive and Brain Sciences, Stephanstr. 1a, 04103 Leipzig, Germany

E-mail: wolters@sci.utah.edu, lgr@mis.mpg.de and wh@mis.mpg.de

Received 11 November 2003
Published 21 May 2004
Online at stacks.iop.org/IP/20/1099
DOI: 10.1088/0266-5611/20/4/007

Abstract

The inverse problem in electro- and magneto-encephalography (EEG/MEG) aims at reconstructing the underlying current distribution in the human brain using potential differences and/or magnetic fluxes that are measured non-invasively directly, or at a close distance, from the head surface. The simulation of EEG and MEG fields for a given dipolar source in the brain using a volume-conduction model of the head is called the forward problem. The finite element (FE) method, used for the forward problem, is able to realistically model tissue conductivity inhomogeneities and anisotropies, which is crucial for an accurate reconstruction of the current distribution. So far, the computational complexity is quite large when using the necessary high resolution FE models. In this paper we will extend the concept of the EEG lead field basis to the MEG and present algorithms for their efficient computation. Exploiting the fact that the number of sensors is generally much smaller than the number of reasonable dipolar sources, our lead field approach will speed up the state-of-the-art forward approach by a factor of more than 100 for a realistic choice of the number of sensors and sources. Our approaches can be applied to inverse reconstruction algorithms in both continuous and discrete source parameter space for EEG and MEG. In combination with algebraic multigrid solvers, the presented approach leads to a highly efficient solution of FE-based source reconstruction problems.

1. Introduction

It is common practice in cognitive research and in clinical routine and research to reconstruct current sources in the human brain by means of non-invasive field measurements outside the head domain. The activity that is measured in EEG and MEG is the result of movements of ions, the so-called *primary currents*, within activated regions in the cortex sheet of the human brain. The primary current can be modelled mathematically by means of a *current dipole* [1–5]. The current dipole causes Ohmic *return currents* to flow through the surrounding medium. The EEG measures the potential differences from the return currents at the scalp surface, whereas the MEG measures the magnetic flux of both primary and return currents. The reconstruction of the dipole sources is called the *inverse problem* of EEG/MEG. Its solution requires the repeated simulation of the field distribution in the head for a given dipole in the brain, the so-called *forward problem*. One of the major advantages of EEG and MEG source reconstruction over other brain imaging techniques such as positron emission tomography (PET) or functional magnetic resonance imaging (fMRI) is its high temporal resolution.

For the forward problem, the volume conductor head has to be modelled. It is known that the head tissue compartments scalp, skull, cerebro-spinal fluid, brain grey matter and white matter have different conductivities and that the layers skull and white matter are anisotropic conductors [6–9]. Different numerical approaches for the forward problem have been used such as multi-layer sphere [10], boundary element (BE) [11–13] and finite element (FE) [4, 14–18] head modelling, where only the FE method is able to treat both realistic geometries and inhomogeneous and anisotropic material parameters. In most cases, magnetic resonance images (MRI) are exploited for the construction of BE and FE head models.

Figure 1 [18] shows an axial cut through a five tissue tetrahedra FE head model with 147 287 nodes and 892 115 elements. The tetrahedra of the layers scalp (light brown), skull (green), cerebro-spinal fluid (light blue), brain grey matter (dark blue) and white matter (yellow) are indicated with different colours. The model was generated by means of a bimodal T1/PD-weighted MRI registration and segmentation approach [18, section 1] followed by a surface-based Delaunay tetrahedrization [18, section 4.7.3]. It is generally assumed that the weak volume currents outside the skull and far away from the EEG and MEG sensors have a negligible influence on the measurements. Therefore, the parts of the head mask lying outside a dilated outer skull surface mask have been cut away when generating the presented volume conductor model. In figure 2 [18], the white matter conductivity anisotropy is shown on the underlying T1-MRI by means of tensor ellipsoids (red) in the barycentres of the white matter finite elements (not shown in the figure).

The influence of skull and white matter conductivity anisotropy on the EEG/MEG forward problem was studied in realistic FE models in [17–20, 21]. In [15, 18, 21, 22], the sensitivity of the EEG inverse problem towards skull conductivity anisotropy was examined. The sensitivity of source reconstruction methods on realistic white matter anisotropy for both EEG and MEG was studied in [18, 22]. In those studies it has been shown that an exact modelling of tissue conductivity inhomogeneity and anisotropy is crucial for an accurate reconstruction of the sources.

An important question is how to handle the computational complexity of FE-modelling with regard to the EEG/MEG inverse problem. It is the state-of-the-art approach for the EEG/MEG inverse methods to solve a forward problem for each possible dipolar source [4, 10–13, 17, 23]. For the FE method, in general, iterative solvers such as the successive over-relaxation (SOR) or the preconditioned conjugate gradient (CG) method with preconditioners such as Jacobi (Jacobi-CG) or incomplete Cholesky (IC-CG) have been used (see, e.g., [4]). In the last few years, algebraic multigrid (AMG) solvers have been developed (see, e.g., [24, 25]).

For the considered application, it was shown in [26] that the AMG, used as a preconditioner for the CG method, is more efficient than IC with or without threshold-techniques. In [27], the AMG solver was found to be superior to an SOR method and to a symmetric SOR preconditioned CG method in finite difference discretizations of the volume conductor. A parallel AMG–CG approach for the forward problem in source localization has been used in [18, 20, 23]. When comparing the parallel AMG–CG on the anisotropic head model shown in figures 1 and 2 with a standard Jacobi-CG on a single processor, speed-up factors of about 80 have been achieved, 10 through multigrid preconditioning and 8 through parallelization on 8 processors [18, 20, 23]. Still, the repeated solution of such a system with a constant geometry matrix for thousands of right-hand sides (the sources) is the major time consuming part within the inverse localization process and limits the resolution of the models.

A further very efficient concept for the reduction of the computational complexity has been described, the concept of reciprocity ([16, 28–30] and [18 section 6.3]). The theory of reciprocity was already introduced in 1853 by [28] and was intensively studied for both the electric and the magnetic cases in [29 sections 11, 12]. The reciprocity theorem for the electric case states that the field of the so-called *lead vectors* is the same as the current field raised by feeding a reciprocal current to the lead [29, section 11.6.3]. The concept allows us to switch the role of the sensors with the dipole locations. For the FE-based EEG source reconstruction, it was shown in [16] how to use this principle for the efficient computation of a so-called *node-oriented lead field basis*, a matrix with 'number sensors' rows and 'number FE nodes' columns. This matrix can then be exploited within the EEG inverse problem. In [30], reciprocity was used for the efficient solution of the EEG inverse problem when using the finite difference method for the forward problem. The application of reciprocity to MEG is nontrivial and has been studied in [31], where the *magnetic lead field theorem* was proved. Nevertheless, as far as we know, it is not yet clear how to efficiently compute the lead field basis for the MEG in combination with the FE method for the forward problem.

In this paper, we will simply apply the mathematical law of associativity with respect to the matrix multiplication. Then, for each head model, we only have to solve 'number of EEG/MEG sensors' times a large sparse FE system of equations in order to compute the lead field basis for both EEG and MEG. This set-up can be computed efficiently using the parallel AMG–CG solver. Each forward solution is then reduced to the multiplication of the lead field basis to a FE right-hand side vector.

The paper is organized as follows: in the next section we describe the electric and the magnetic forward problems. In section 3, FE discretization aspects are discussed. Section 4 contains a brief description of inverse methods on discrete [12, 32–37] and on continuous [11, 18, 38] source parameter space. In section 5, we estimate the complexity of the state-of-the-art approach to the EEG/MEG inverse problem. Section 6 contains our new approach resulting in two algorithms that solve the EEG and MEG inverse problem. In section 7, we will discuss the applicability of the mathematical dipole model in combination with the subtraction method in the context of our new approach. Finally, we conclude and give some perspectives in section 8.

2. Forward problem formulation

2.1. The Maxwell equations

Let us begin with the introduction of some notation: let $\mathbf{E}$ and $\mathbf{D}$ be the electric field and electric displacement, respectively, ρ the electric free charge density, ϵ the electric permeability and $\mathbf{j}$

the electric current density. By μ we denote the magnetic permeability and by **H** and **B** the magnetic field and induction, respectively.

In the considered low frequency band (frequencies below 2000 Hz), the capacitive component of tissue impedance, the inductive effect and the electromagnetic propagation effect and thus the temporal derivatives can be neglected in the Maxwell equations of electrodynamics [39]. It can be assumed that μ is constant over the whole volume and is equal to the permeability of vacuum [39]. Therefore, the electric and magnetic fields can be described by the quasi-static Maxwell equations

$$\begin{aligned} &\operatorname{div} \mathbf{D} = \rho \\ &\operatorname{curl} \mathbf{E} = 0 \\ &\operatorname{curl} \mathbf{B} = \mu \mathbf{j} \qquad (1) \\ &\operatorname{div} \mathbf{B} = 0 \qquad (2) \end{aligned}$$

with the material equations

$$\begin{aligned} &\mathbf{D} = \epsilon \mathbf{E} \\ &\mathbf{B} = \mu \mathbf{H}, \end{aligned}$$

since biological tissue mainly behaves as an electrolyte [39]. The electric field can be expressed as a negative gradient of a scalar potential,

$$\mathbf{E} = -\operatorname{grad} \mathrm{u}. \qquad (3)$$

The current density is generally divided into two parts [39], the so-called *primary* or impressed current, $\mathbf{j}^p$, and the *secondary* or return currents, $\underline{\underline{\sigma}}\mathbf{E}$,

$$\mathbf{j} = \mathbf{j}^p + \underline{\underline{\sigma}}\mathbf{E}, \qquad (4)$$

where $\underline{\underline{\sigma}}$ denotes the 3×3 conductivity tensor. The sources to be localized during the inverse problem and to be modelled in the forward problem, the primary currents $\mathbf{j}^p$, are movements of ions within the dendrites of the large pyramidal cells of activated regions in the cortex sheet of the human brain. Stimulus-induced activation of a large number of excitatory synapses of a whole pattern of neurons leads to negative current monopoles under the brain surface and to positive monopoles quite closely underneath. Various modelling possibilities for the primary currents are discussed in the literature [1–5]. While the so-called *mathematical dipole model* [2, 18] will be considered later in section 7, we will restrict ourselves in the following to the *blurred dipole model* [4, 18].

2.2. The electric forward problem

We now assume that the conductivity distribution $\underline{\underline{\sigma}}$ in the head domain is given. Taking the divergence of equation (1) (divergence of a curl of a vector is zero) and using equations (3) and (4) gives the equation

$$-\operatorname{div}(\underline{\underline{\sigma}} \operatorname{grad} \mathrm{u}) = -\operatorname{div} \mathbf{j}^p \qquad \text{in } \Omega, \qquad (5)$$

which describes the potential distribution in the head domain Ω due to a primary current $\mathbf{j}^p$ in the brain. For the forward problem, the primary current and the conductivity distribution in the volume conductor are known, and the equation has to be solved for the unknown potential distribution. The boundary condition

$$(\underline{\underline{\sigma}}_1 \operatorname{grad} \mathrm{u}_1, \mathbf{n})|_{\text{at surface}} = (\underline{\underline{\sigma}}_2 \operatorname{grad} \mathrm{u}_2, \mathbf{n})|_{\text{at surface}}$$

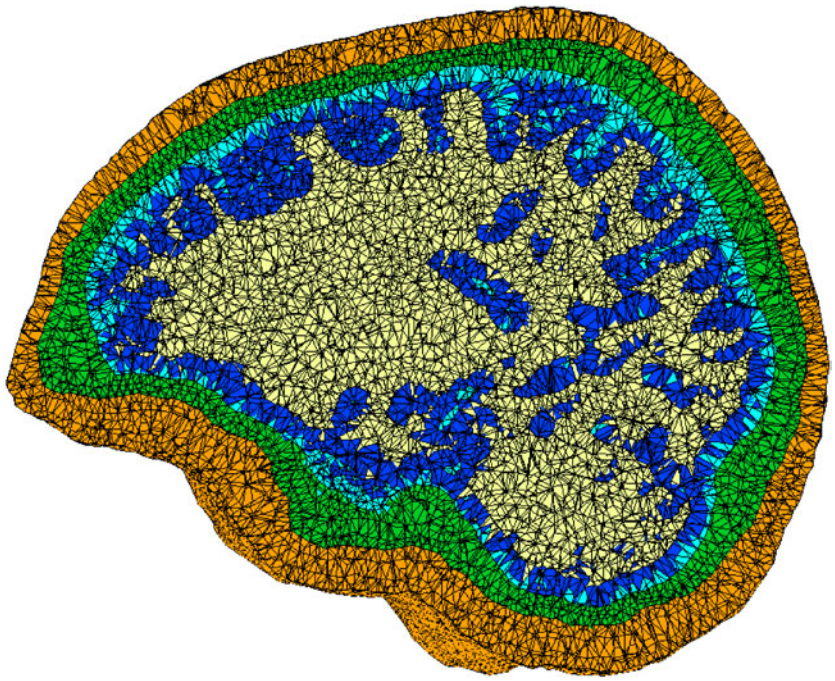

Figure 1. Five tissue FE head model with 147 287 nodes and 892 115 elements. The tetrahedra of the layers scalp, skull, cerebro-spinal fluid, brain grey matter and white matter are indicated with different colors.

with $\mathbf{n}$ the unit surface normal expresses the continuity of the current density across any surface between regions of different conductivity. We find homogeneous Neumann conditions on the head surface $\Gamma = \partial\Omega$,

$$(\underline{\underline{\sigma}}\,\mathrm{grad}\,\mathrm{u}, \mathbf{n})|_{\Gamma} = 0, \tag{6}$$

and, additionally, a reference electrode with given potential, i.e.,

$$\mathrm{u}_{\mathrm{ref}} = 0. \tag{7}$$

2.3. The magnetic forward problem

Since the divergence of $\mathbf{B}$ is zero (see Maxwell equation (2)), a magnetic potential $\mathbf{A}$ with $\mathbf{B} = \mathrm{curl}\,\mathbf{A}$ can be introduced and, using Coulomb's gauge $\mathrm{div}\,\mathbf{A} = 0$, Maxwell's equation (1) transforms to

$$\mu(\mathbf{j}^p - \underline{\underline{\sigma}}\,\mathrm{grad}\,\mathrm{u}) = \mathrm{curl}\,(\mathrm{curl}\,\mathbf{A}) = \mathrm{grad}\,(\mathrm{div}\,\mathbf{A}) - \Delta\mathbf{A} = -\Delta\mathbf{A}.$$

The source term is vanishing outside the volume conductor, so that the solution of this Poisson equation is given by [40]

$$\mathbf{A}(\mathbf{x}) = \frac{\mu}{4\pi}\int_{\Omega}\frac{\mathbf{j}^p(\mathbf{y}) - \underline{\underline{\sigma}}(\mathbf{y})\mathrm{grad}\,\mathrm{u}(\mathbf{y})}{|\mathbf{x}-\mathbf{y}|}\,\mathrm{d}\mathbf{y}. \tag{8}$$

Let F be the surface enclosed by the MEG magnetometer flux transformer $\Upsilon = \partial F$. A typical MEG magnetometer conduction loop Υ is shown in figure 3(b). The magnetic flux Ψ through Υ is determined as a surface integral over the magnetic induction for the coil area F, or, using

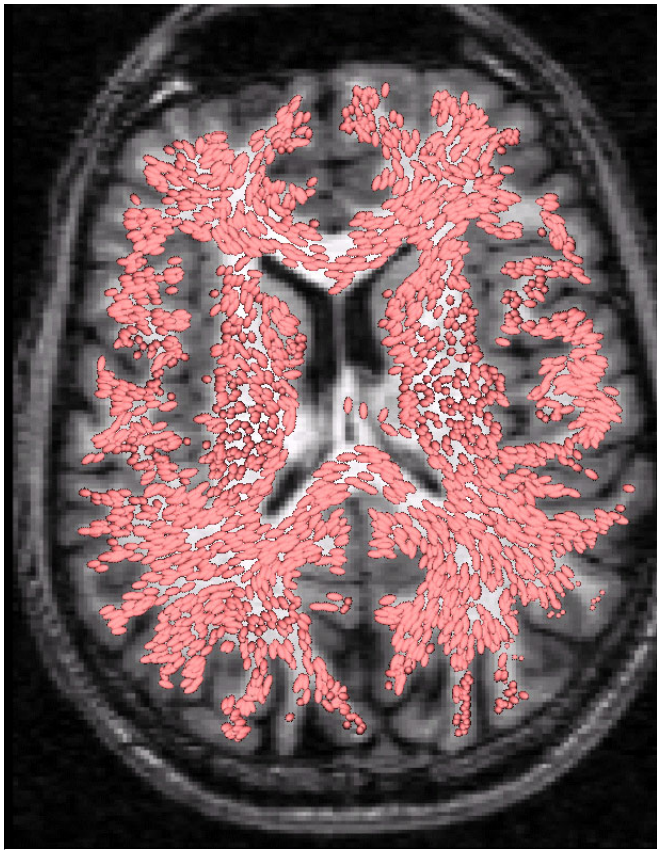

Figure 2. White matter anisotropy modelled with conductivity tensor ellipsoids in the barycentres of the white matter finite elements presented on an underlying magnetic resonance image.

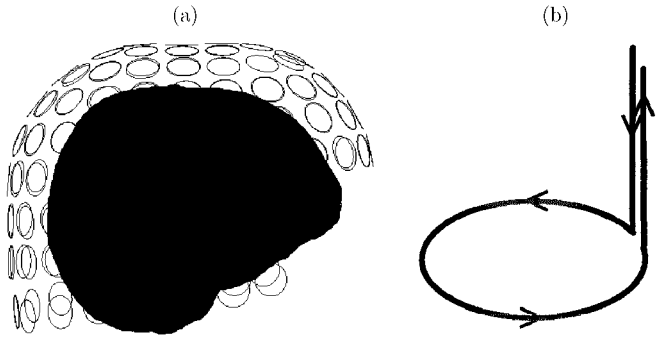

Figure 3. (a) Sensors of whole head BTI-148-channel MEG system together with the outer surface of the head model of figure 1 [18]. (b) A typical magnetometer flux transformer.

the Stokes theorem [40], as

$$\Psi = \int_F \mathbf{B} \cdot \mathrm{d}\mathbf{f} = \oint_\Upsilon \mathbf{A}(\mathbf{x}) \cdot \mathrm{d}\mathbf{x} \overset{(8)}{=} \oint_\Upsilon \frac{\mu}{4\pi} \int_\Omega \frac{\mathbf{j}^p(\mathbf{y})}{|\mathbf{x}-\mathbf{y}|}\,\mathrm{d}\mathbf{y} \cdot \mathrm{d}\mathbf{x} + \oint_\Upsilon \frac{\mu}{4\pi} \int_\Omega \frac{-\underline{\underline{\sigma}}(\mathbf{y})\,\mathrm{grad}\,\mathrm{u}(\mathbf{y})}{|\mathbf{x}-\mathbf{y}|}\,\mathrm{d}\mathbf{y} \cdot \mathrm{d}\mathbf{x}.$$

The first part of this magnetic flux is called the *primary magnetic flux* and in the following denoted with Ψ_p, and the second is the so-called *secondary magnetic flux* Ψ_{sec}.

Ψ_p is only dependent on the source model and can in general be computed by simply evaluating an analytical formula [11, 18, 41, 42].

If we define

$$\mathbf{C}(\mathbf{y}) = \oint_{\Upsilon} \frac{1}{|\mathbf{x}-\mathbf{y}|}\,\mathrm{d}\mathbf{x}, \tag{9}$$

and if the potential distribution u is given, the final equation for Ψ_{sec} emerges from the secondary (return) currents and can be given by

$$\Psi_{\text{sec}} = -\frac{\mu}{4\pi}\int_{\Omega} (\underline{\underline{\sigma}}(\mathbf{y})\text{grad}\,\mathrm{u}(\mathbf{y}), \mathbf{C}(\mathbf{y}))\,\mathrm{d}\mathbf{y}. \tag{10}$$

3. Discretization aspects for the forward problem

3.1. Discretizing the electric forward problem

For the numerical solution, we choose a finite-dimensional subspace with dimension N and a standard nodal finite element basis $\psi_1, \ldots, \psi_N$. The numerical solution process depends on the chosen model for the primary source. Here, we will refer to the literature for a deeper discussion and restrict ourselves to the following remarks.

The mathematical dipole model together with the subtraction approach [14, 18, 43] will be discussed later in section 7.

The blurred dipole model [4, 18] follows the law of St Venant and is made up from monopolar loads on all neighbouring FE nodes so that the dipolar moment is fulfilled and the source load is as regular as possible. The dipole moment is then only a means for visualization. In this case, variational and FE techniques can be directly applied to equation (5) with boundary conditions (6) and reference potential (7). This yields a system of linear equations

$$\begin{array}{c} N \\ \end{array}\begin{array}{|c|}\hline \\ \mathsf{K} \\ \\ \hline \end{array}\begin{array}{c} \\ \cdot \\ \\ N \end{array}\begin{array}{|c|}\hline \\ \\ \\ \hline \end{array} = \begin{array}{|c|}\hline \\ \\ \\ \hline \end{array} \qquad \mathsf{K}\underline{\mathrm{u}} = \underline{\mathrm{j}}^{\text{blur}} \tag{11}$$

where the stiffness or geometry matrix has entries

$$\mathsf{K}_{ij} = \int_{\Omega} (\text{grad}\,\psi_j(\mathbf{y}), \underline{\underline{\sigma}}(\mathbf{y})\text{grad}\,\psi_i(\mathbf{y}))\,\mathrm{d}\mathbf{y} \qquad \forall 1 \leqslant i, j \leqslant N \tag{12}$$

and is symmetric positive definite. The positive definiteness follows from the ellipticity of the underlying bilinear form [18]. The right-hand-side $\underline{\mathrm{j}}^{\text{blur}}$ has only c_{nz} non-zero entries, if c_{nz} is the number of neighbouring FE nodes to that FE node which is closest to the location of the dipole. The vector $\underline{\mathrm{u}} \in \mathbb{R}^N$ denotes the solution vector for the total potential.

Let us further assume that the $(s_{\text{eeg}} - 1)$ non-reference EEG electrodes directly correspond to FE nodes at the surface of the head model. It is then easy to determine a restriction matrix $\mathsf{R} \in \mathbb{R}^{(s_{\text{eeg}}-1)\times N}$, which has only one non-zero entry with the value 1 in each row and which

maps the potential vector onto the non-reference EEG electrodes

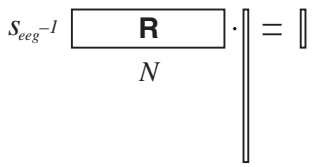

$$\mathsf{R}\underline{u} =: \underline{u}_{\text{eeg}}. \tag{13}$$

3.2. Discretizing the magnetic forward problem

For the magnetic forward problem, the flux transformers of the MEG device have to be modelled (see equation (9)). As an example, the sensors of the whole head BTI-148-channel MEG system together with the outer surface of the head model of figure 1 are shown in figure 3(a). A typical magnetometer coil Υ is shown in figure 3(b). Following [42], we model such a coil by means of a thin, closed conductor loop, using isoparametric quadratic row elements. When approximating the potential u by means of its Galerkin projection, equation (10) can be written in matrix form

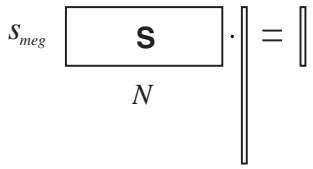

$$\mathsf{S}\underline{u} =: \underline{\Psi}_{\text{sec}} \tag{14}$$

with $\mathsf{S} \in \mathbb{R}^{s_{\text{meg}} \times N}$ the so-called *secondary flux matrix*. S maps the potential onto the secondary flux vector $\underline{\Psi}_{\text{sec}} \in \mathbb{R}^{s_{\text{meg}}}$. The secondary flux matrix has the entries

$$\mathsf{S}_{ij} = -\frac{\mu}{4\pi} \int_{\Omega} (\underline{\underline{\sigma}}(\mathbf{y}) \text{grad}\, \psi_j(\mathbf{y}), \mathbf{C}_i(\mathbf{y}))\, \mathrm{d}\mathbf{y} \qquad \forall 1 \leqslant j \leqslant N$$

where $\mathbf{C}_i(\mathbf{y})$ denotes the function (9) for the ith MEG magnetometer Υ_i $(1 \leqslant i \leqslant s_{\text{meg}})$. For the computation of the matrix entries of S, a FE ansatz for the integrand and Gauss integration is used [42].

4. The inverse problem

The non-uniqueness of the inverse problem in EEG and MEG implies that assumptions on the source model, as well as anatomical and physiological *a priori* knowledge about the source region, should be taken into account to obtain a unique solution.

In the following, we will distinguish two classes of inverse methods, those in *discrete source parameter space* and those in *continuous source parameter space*. The dipole model for the primary current is regarded as the 'atomic' structure for both classes.

4.1. Inverse methods for a discrete source parameter space

One piece of physiological *a priori* information about the source region (*influence space*) is the assumption that the generators must be located on the folded surface of the brain inside the cortex, ignoring white matter and deeper structures such as basal ganglia, brain stem and cerebellum. If convolutions of the cortical surface are appropriately modelled by the segmentation procedure, another addition is the anatomical information that the generators are perpendicular to this surface [3, 44]. This limitation to normally oriented dipoles is called the *normal-constraint*. Because the dipole models an active source region with a certain extent

and the resolution of the inverse current reconstruction by means of noisy EEG or MEG data is limited, most inverse methods (see, e.g., [12, 32–37]) and especially all so-called *current density methods* [12, 32, 36, 37] are based on a discretized influence space. The discretization can be represented, for example, by the vertices of a cortical triangulation when using the physiological constraint. Other approaches use regular 3D discretizations of the whole brain volume. The so-called *influence nodes* are the n_{inf} vertices of the discretized influence space. Since the differential equation is linear, it is possible to set up a so-called *influence matrix* $\mathrm{L} \in \mathbb{R}^{\mathrm{s}\times\mathrm{r}}$ (often also called *lead field matrix*). A forward solution for a dipole on one of the n_{inf} influences nodes with unit strength in one Cartesian direction at the

$$\mathrm{s} = s_{\mathrm{eeg}} + s_{\mathrm{meg}}$$

EEG/MEG measurement sensors is stored as a column of L. If the physiological *a priori* information and the normal-constraint are applied, there is only one possible dipole direction for each influence node and thus every dipole location $i \in \{1, \ldots, n_{\mathrm{inf}}\}$ is represented by only one column in the influence matrix, i.e. $\mathrm{r} = n_{\mathrm{inf}}$. For the unconstrained case, three columns in L represent the three orthogonal unit dipoles at a specific location, i.e. $\mathrm{r} = 3n_{\mathrm{inf}}$.

If once, the discretization of the influence space has been fixed, the block of the r right-hand sides $\underline{j}^{\mathrm{blur}} \in \mathbb{R}^N$ (see section 7 for the mathematical dipole model) can be set up. The goal is then a fast computation of the influence matrix L, which can subsequently be used for the whole variety of inverse reconstruction methods for discrete source parameter space.

4.2. Inverse methods for a continuous source parameter space

The second class of inverse methods exploits a continuous source parameter space [11, 18, 38]. One could imagine, for example, the restriction of the inverse reconstruction to a limited number of dipoles (with respect to the application: one up to three). Their nonlinear location parameters are optimized continuously in the brain volume, while the remaining parameters are determined with a linear fit to the measured EEG/MEG data within each optimization step. This is done, e.g., within the so-called *dipole fit methods* [11, 18, 38]. The number r of necessary forward simulations in such methods is dependent on the convergence speed of the optimization method. This class of inverse algorithms cannot exploit the influence matrix concept (apart from interpolation techniques [13]), since the new dipole parameters and thus the new right-hand sides are only determined within the previous optimization step. Still, we can apply our new approach successfully.

5. State-of-the-art approach in EEG/MEG source reconstruction

For the considered inhomogeneous and anisotropic volume conductor models, the AMG–CG iterative solver [18, 20, 23, 26] turned out to be an asymptotically optimal solver method for the numerical solution of (11), where the operation count and memory demand are of the order $\mathcal{O}(N)$. Our approach can also be applied in combination with other solver methods, but in the following we will only consider the AMG–CG.

We will now describe the state-of-the-art approach for the EEG/MEG inverse problem which covers both classes of inverse methods. A new FE right-hand side vector is determined by the inverse algorithm, and the AMG–CG solver is used for the numerical solution of the potential distribution. For the computation of the secondary flux at the MEG-sensors, the potential distribution is then multiplied by the secondary flux matrix following equation (14). The restriction (13) terminates the forward computation.

The numerical tests are performed on a Sun Ultrasparc III with 900 MHz CPU clock rate. We only use a single processor for the following computations.

5.1. Complexity estimation for AMG–CG solver

We first estimate the complexity for an AMG–CG solution [23], following the MultiGrid operation count of [45, section 10.4.4]. With $c_{nz} * N$ being the sparsity of the geometry/stiffness matrix, we assume $C_S * c_{nz} * N$ operations for the smoother, $C_D * c_{nz} * N$ for the computation of defect and restriction and $C_P * N$ for the prolongation of the error. Here, C_S denotes the cost factor for the smoother which is an iteration-specific constant. We use Gauss–Seidel smoothing for which it is $C_S = 2 - 2/c_{nz}$ [45, section 4.6.1]. C_P and C_D depend on the chosen prolongation operator. As described in [23], our prolongation matrix interpolates the value of a fine grid node (which is not at the same time a coarse grid node) only from strong neighbour coarse grid nodes, i.e. $C_P \ll c_{nz}$. In our application, the restriction matrix is the transpose of the prolongation matrix. We use a V-cycle with only one pre- and one post-smoothing step within each preconditioning operation. We then obtain as an approximation of the necessary work for the MG preconditioner [45, theorem 10.4.2]:

$$\tfrac{8}{7} * (2 * C_S + C_D + C_P/c_{nz}) * c_{nz} * N.$$

We furthermore have to count one matrix-vector multiplication ($2 * c_{nz} * N$ operations), two scalar products ($2 * 2 * N$ operations) and three vector additions ($3 * N$ operations) for the CG step. If we assume that i iterations have to be carried out, we will need for one AMG–CG solution approximately $i * k * N$ operations with

$$k := \tfrac{8}{7} * (2 * C_S + C_D + 2 + (C_P + 7)/c_{nz}) * c_{nz}.$$

We will study the head model of figures 1 and 2 with $N = 147\,287$ FE nodes as an example: in order to reach a sufficient accuracy, we have to reduce the relative error by a factor of 10^8 which can be accomplished by $i = 20$ iterations of AMG–CG [18, 20, 23, 26]. On our machine, each iteration takes 1.269 s, i.e. 25.38 s to solve for each right-hand side.

5.2. Complexity estimation for the state-of-the-art approach

Let us now have a look at the complexity of the state-of-the-art approach for the inverse problem.

For the matrix-vector multiplication in equation (14), $2 * s_{\text{meg}} * N$ operations are needed. Let us neglect the work for the restriction $\underline{\mathrm{u}}_{\text{eeg}} = \mathsf{R}\underline{\mathrm{u}}$ and for the computation of the FE right-hand side vector. Then, for each inverse algorithm with r different right-hand sides, the state-of-the-art approach needs

$$\mathrm{r} * ((i * k + 2 * s_{\text{meg}}) * N)$$

operations.

In EEG/MEG source reconstruction, r is generally quite large, especially because the results of various different inverse algorithms based on different hypotheses on the underlying current distribution are compared to each other. Already an anatomically correct discretization of the cortical surface, respecting all curvatures of the cortical sulci and gyri, results in at least 10^4 influence nodes [18, figure 2.5]. This number would be even exceeded in the case of a 3D discretization of the whole brain volume. In contrast to that, the number of sensors s is rather small. The most modern vector-MEG devices have at most 500 sensors and for the EEG, not more than 150 sensors can be fixed on the head surface. In most applications, the number of sensors is below 150 (see figure 3(a)) as an example).

In our model problem, we have $s_{\text{meg}} = 150$ sensors and $\mathrm{r} = 30\,357$ right-hand sides (possible dipoles). The solution of the FE system for 30 357 right-hand sides and subsequent matrix-vector multiplication with S from equation (14) takes

$$774\,331\,\mathrm{s} = 215\,\mathrm{h},$$

which is too expensive for realistic applications. In the next section, we explain how one can severely reduce this complexity, down to 1 h.

6. Computation of the lead field basis and influence matrix

The inverse of the geometry/stiffness matrix, K^{-1}, exists, but its computation is a difficult task, since the sparseness of K will be lost while inverting. But with regard to the EEG inverse problem, we are only interested in computing

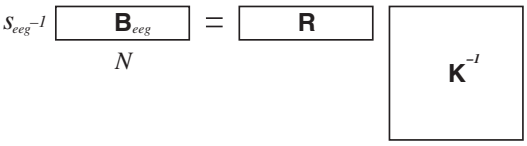

$$\mathsf{B}_{\mathrm{eeg}} := \mathsf{R}\mathsf{K}^{-1} \in \mathbb{R}^{(s_{\mathrm{eeg}}-1)\times N}, \tag{15}$$

which describes the direct mapping of a FE right-hand side vector to the non-reference electrodes:

$$\mathsf{B}_{\mathrm{eeg}}\underline{\mathsf{j}}^{\mathrm{blur}} \overset{(15)}{=} \mathsf{R}\mathsf{K}^{-1}\underline{\mathsf{j}}^{\mathrm{blur}} \overset{(11)}{=} \mathsf{R}\underline{\mathsf{u}} \overset{(13)}{=} \underline{\mathsf{u}}_{\mathrm{eeg}}.$$

Weinstein *et al* [16] introduced the notation *EEG lead field basis* for $\mathsf{B}_{\mathrm{eeg}}$. We will now see that we face a comparable situation with regard to the MEG inverse problem. In fact, let us define the *MEG lead field basis*:

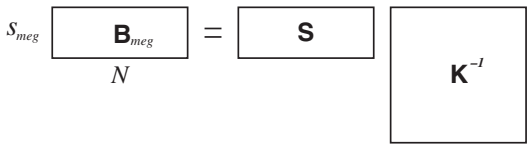

$$\mathsf{B}_{\mathrm{meg}} := \mathsf{S}\mathsf{K}^{-1} \in \mathbb{R}^{s_{\mathrm{meg}}\times N}. \tag{16}$$

One should note that the rows of $\mathsf{B}_{\mathrm{eeg}}$ do indeed form a basis in the mathematical sense, while this is not necessarily true for $\mathsf{B}_{\mathrm{meg}}$. $\mathsf{B}_{\mathrm{meg}}$ describes the direct mapping of the FE right-hand side vector to the secondary magnetic flux vector:

$$\mathsf{B}_{\mathrm{meg}}\underline{\mathsf{j}}^{\mathrm{blur}} \overset{(16)}{=} \mathsf{S}\mathsf{K}^{-1}\underline{\mathsf{j}}^{\mathrm{blur}} \overset{(11)}{=} \mathsf{S}\underline{\mathsf{u}} \overset{(14)}{=} \underline{\Psi}_{\mathrm{sec}}.$$

The lead field basis can be computed as follows: if we multiply the matrix equation

$$\begin{bmatrix}\mathsf{B}_{\mathrm{eeg}}\\ \mathsf{B}_{\mathrm{meg}}\end{bmatrix} = \begin{bmatrix}\mathsf{R}\\ \mathsf{S}\end{bmatrix}\mathsf{K}^{-1}$$

with K from the right-hand side and transpose both sides, we obtain

$$\mathsf{K}\begin{bmatrix}\mathsf{B}_{\mathrm{eeg}}^{\mathrm{tr}} & \mathsf{B}_{\mathrm{meg}}^{\mathrm{tr}}\end{bmatrix} = [\mathsf{R}^{\mathrm{tr}} \quad \mathsf{S}^{\mathrm{tr}}].$$

The last step uses the symmetry of the geometry matrix (see equation (12)).

Algorithm 1 INVERSE PROBLEM WITH MODERATE SIZE OF THE LEAD FIELD BASIS

Precompute $\mathsf{B}_{\mathrm{eeg}}$ and $\mathsf{B}_{\mathrm{meg}}$ and store both matrices
repeat
INVERSE ALGORITHM COMPUTES NEW $\underline{\mathsf{j}}^{\mathrm{blur}}$
MULTIPLY $\underline{\mathsf{j}}^{\mathrm{blur}}$ BY $\mathsf{B}_{\mathrm{eeg}}$ AND $\mathsf{B}_{\mathrm{meg}}$: USE SPECIAL STRUCTURE OF $\underline{\mathsf{j}}^{\mathrm{blur}}$
until TERMINATION OF INVERSE ALGORITHM

Algorithm 2 INVERSE PROBLEM WITH LARGE SIZE OF THE LEAD FIELD BASIS

PRECOMPUTE $\mathrm{J}^{\mathrm{blur}} \in \mathbb{R}^{N\times \mathrm{r}}$ IN CSC-FORMAT
for $\mathrm{i} = 1, \ldots, \mathrm{s}$ **do**
  DETERMINE THE iTH ROW OF THE LEAD FIELD BASIS
  MULTIPLY THIS ROW BY $\mathrm{J}^{\mathrm{blur}}$, I.E., COMPUTE iTH ROW OF L
  STORE iTH ROW IN $\mathrm{L} \in \mathbb{R}^{\mathrm{s}\times \mathrm{r}}$
end for
USE L FOR INVERSE METHODS ON DISCRETE PARAMETER SPACE

6.1. Algorithms

Let us first assume that we are equipped with a computer memory which is large enough to store $\mathrm{s} * N$ doubles for the lead field bases $\mathsf{B}_{\mathrm{eeg}}$ and $\mathsf{B}_{\mathrm{meg}}$. In this case, algorithm 1 can be used. In a set-up phase, $\mathsf{B}_{\mathrm{eeg}}$ and $\mathsf{B}_{\mathrm{meg}}$ are computed once per head-model by means of solving s large sparse FE-systems of equations using, e.g., the iterative AMG-CG solver. The lead field bases can then be exploited for any new FE right-hand side within the inverse algorithm for both classes of inverse methods, discrete and continuous. Remember that for the blurred dipole model, $\underline{\mathrm{j}}^{\mathrm{blur}}$ has only c_{nz} non-zero entries, which can efficiently be used within the matrix-vector multiplication.

The mathematical dipole would lead to dense right-hand side vectors (no non-zero entries). In this case, we suggest special techniques described in section 7.

If the computer memory is too small to store $\mathrm{s} * N$ doubles for $\mathsf{B}_{\mathrm{eeg}}$ and $\mathsf{B}_{\mathrm{meg}}$ and if only inverse methods for discrete source parameter space in combination with the blurred dipole model are of interest, algorithm 2 is the appropriate one. In a set-up phase, the block with r right-hand sides $\underline{\mathrm{j}}^{\mathrm{blur}}$ for all blurred dipoles of the influence space is precomputed and stored using a compressed sparse column (CSC) format [46]. Let us denote this matrix with $\mathrm{J}^{\mathrm{blur}} \in \mathbb{R}^{N\times \mathrm{r}}$. Each row of the lead field basis can then be computed using AMG-CG and directly multiplied to $\mathrm{J}^{\mathrm{blur}}$. The result is a row of the influence matrix $\mathrm{L} \in \mathbb{R}^{\mathrm{s}\times \mathrm{r}}$ from chapter 4.1. L can then be exploited by means of all inverse methods working on that specific discrete influence space.

6.2. Complexity of algorithms 1 and 2

Let us now have a look at the complexity of algorithm 1 that computes the lead field bases $\mathsf{B}_{\mathrm{eeg}}$ and $\mathsf{B}_{\mathrm{meg}}$.

As in section 5.2 we consider the tetrahedra model problem (figures 1 and 2) with $\mathrm{r} = 30\,357$ right-hand sides and $\mathrm{s} = s_{\mathrm{meg}} = 150$ sensors. In brackets we give the concrete time for the computations on our machine (cf section 6).

After a set-up with

$$\mathrm{s} * i * k * N \text{ operations} \qquad (3807 \text{ s}),$$

which is a unique calculation for each individual head geometry, we only have to multiply the new FE right-hand side vector by the lead field bases. For r full right-hand side vectors, this amounts to

$$\mathrm{r} * (2 * \mathrm{s} * N) \text{ operations} \qquad (3871 \text{ s}).$$

If, furthermore, the blurred dipole is used, this operation count is reduced to only

$$\mathrm{r} * (2 * \mathrm{s} * c_{nz}) \text{ operations} \qquad (4.7 \text{ s})$$

for each inverse method. Note that this number is independent of the mesh-resolution. The overall complexity in this case is

$$\mathrm{s} * i * k * N + 2 * \mathrm{r} * \mathrm{s} * c_{nz} \qquad (3812\ \mathrm{s}),$$

i.e. it is mainly determined by the set-up phase. The complexity of algorithm 2 is the same (if the blurred dipole is used). The overall complexity of our approach is thus by a factor r/s (in our model problem: 200) smaller than the complexity for the state-of-the-art approach. If various inverse methods are compared to each other, this factor will grow with the number r of FE right-hand sides.

7. Mathematical dipole and subtraction approach

For the mathematical dipole [14, 18, 43], a subtraction approach is used for the solution of the electric forward problem. The total potential u is split into two parts, the singularity potential u^∞ corresponding to the location of the dipole, $y \in \mathbb{R}^3$, with the dipole moment $M(y) \in \mathbb{R}^3$ [41],

$$\mathrm{u}^\infty(x) := \frac{1}{4\pi} \frac{\langle M(y), x - y \rangle}{\|x - y\|^3}, \qquad \operatorname{div} \operatorname{grad} \mathrm{u}^\infty = J^p := \operatorname{div} M(y) \delta(x - y) \tag{17}$$

and the unknown *correction potential* $\mathrm{u}^{\mathrm{corr}}$:

$$\mathrm{u} = \mathrm{u}^\infty + \mathrm{u}^{\mathrm{corr}}.$$

A FE ansatz for the correction potential leads to a linear system of equations

$$\mathsf{K} \underline{\mathrm{u}}^{\mathrm{corr}} = \underline{\mathrm{j}}^{\mathrm{corr}} \tag{18}$$

with the same geometry matrix K as in (12). The right-hand side $\underline{\mathrm{j}}^{\mathrm{corr}} \in \mathbb{R}^N$ is a full vector and $\underline{\mathrm{u}}^{\mathrm{corr}} \in \mathbb{R}^N$ denotes the solution vector for the correction potential. A precise definition of the right-hand side is

$$\underline{\mathrm{j}}^{\mathrm{corr}} = (\mathsf{K}_\Delta - \mathsf{K} + \mathsf{K}_\mathrm{n}) \underline{\mathrm{u}}^\infty. \tag{19}$$

K_Δ is the discrete Laplacian and K_n the discretization of the inhomogeneous Neumann boundary conditions at the surface of the volume conductor induced by u^∞ (see, e.g., [18, sections 4.4.1, 4.7.4]). The sparsity pattern of both matrices, K_Δ and K_n, is contained in the sparsity pattern of K. Therefore, $c_{nz} * N$ is also the sparsity of $\mathsf{K}_\Delta + \mathsf{K}_\mathrm{n}$.

The restriction matrix R from (13) maps the potential vector onto the potential of the non-reference EEG electrodes

$$\underline{\mathrm{u}}_{\mathrm{eeg}} := \mathsf{R}(\underline{\mathrm{u}}^{\mathrm{corr}} + \underline{\mathrm{u}}^\infty) \overset{(18)}{=} \mathsf{R}\mathsf{K}^{-1} \underline{\mathrm{j}}^{\mathrm{corr}} + \mathsf{R}\underline{\mathrm{u}}^\infty \overset{(19)}{=} \mathsf{R}\mathsf{K}^{-1}(\mathsf{K}_\Delta + \mathsf{K}_\mathrm{n}) \underline{\mathrm{u}}^\infty. \tag{20}$$

Equation (14) then gets

$$\underline{\Psi}_{\mathrm{sec}} := \mathsf{S}(\underline{\mathrm{u}}^{\mathrm{corr}} + \underline{\mathrm{u}}^\infty) \overset{(18)}{=} \mathsf{S}\mathsf{K}^{-1} \underline{\mathrm{j}}^{\mathrm{corr}} + \mathsf{S}\underline{\mathrm{u}}^\infty \overset{(19)}{=} \mathsf{S}\mathsf{K}^{-1}(\mathsf{K}_\Delta + \mathsf{K}_\mathrm{n}) \underline{\mathrm{u}}^\infty. \tag{21}$$

Algorithm 3 INVERSE PROBLEM WITH CONTINUOUS SOURCE PARAMETER SPACE

Precompute $\mathsf{B}^\infty_{\mathrm{eeg}}$ and $\mathsf{B}^\infty_{\mathrm{meg}}$ and store both matrices
repeat
  INVERSE ALGORITHM COMPUTES NEW $\underline{\mathrm{u}}^\infty$
  MULTIPLY $\underline{\mathrm{u}}^\infty$ BY $\mathsf{B}^\infty_{\mathrm{eeg}}$ AND $\mathsf{B}^\infty_{\mathrm{meg}}$
until TERMINATION OF INVERSE ALGORITHM

The matrices

$$\mathsf{B}_{\mathrm{eeg}}^{\infty} := \mathsf{R}\mathsf{K}^{-1}(\mathsf{K}_{\Delta} + \mathsf{K}_{\mathrm{n}}) \in \mathbb{R}^{(s_{\mathrm{eeg}}-1)\times N}$$

and

$$\mathsf{B}_{\mathrm{meg}}^{\infty} := \mathsf{S}\mathsf{K}^{-1}(\mathsf{K}_{\Delta} + \mathsf{K}_{\mathrm{n}}) \in \mathbb{R}^{s_{\mathrm{meg}}\times N}$$

can be precomputed and used for any right-hand side $\underline{\mathrm{u}}^{\infty}$ coming either from a discrete or a continuous source parameter space.

7.1. Algorithms and complexity for the mathematical dipole

In the following we give in brackets the concrete times for the computations on our machine (cf section 5.2) for the tetrahedra model problem (figures 1 and 2).

For a continuous source parameter space algorithm 3 is applicable. Here, one has to precompute $\mathsf{B}_{\mathrm{eeg}}^{\infty}$ and $\mathsf{B}_{\mathrm{meg}}^{\infty}$ with a complexity of

$$\mathrm{s} * i * k * N + \mathrm{s} * c_{nz} * N \qquad (3876\ \mathrm{s})$$

and can then use these matrices to compute $\underline{\mathrm{u}}_{\mathrm{eeg}}$ and $\underline{\Psi}_{\mathrm{sec}}$ with a complexity of $\mathrm{s} * N$ (0.1 s) for each dipole (i.e. for each $\underline{\mathrm{u}}^{\infty}$). For a total of $\mathrm{r} = 30\,357$ dipoles this complexity is

$$\mathrm{r} * (2 * \mathrm{s} * N) \qquad (3871\ \mathrm{s}).$$

The total complexity for both set-up and solution phase is

$$(i * k + c_{nz} + 2 * \mathrm{r}) * \mathrm{s} * N \text{ operations} \qquad (7747\ \mathrm{s}),$$

which is 100 times less than the complexity for the state-of-the-art approach.

For a discrete source parameter space the r possible dipole locations are known. In this case we can use the same strategy as for the blurred dipole, namely to store the whole matrix U^{∞} whose columns are the vectors $\underline{\mathrm{u}}^{\infty}$ for the respective dipole locations. However, the matrix U^{∞} is not sparse. A new technique to store matrices of this type in a data-sparse form are so-called hierarchical matrices, or short $\mathcal{H}$-matrices [47–50]. This format exploits the fact that the function $\mathrm{u}^{\infty}(x)$ can be interpolated efficiently. The dependence of $\mathrm{u}^{\infty}(x)$ on the dipole location y is complicated, but we can split the function u^{∞} into

$$\mathrm{u}^{\infty}(x) = \sum_{i=1}^{3} \frac{M(y)_i}{4\pi} \cdot \frac{(x_i - y_i)}{\|x - y\|^3},$$

such that only the term $(x_i - y_i)/\|x - y\|^3$ has to be interpolated, i.e. we have to fulfil the standard *admissibility condition*

$$\min\{\mathrm{diam}(X), \mathrm{diam}(Y)\} \leqslant \mathrm{dist}(X, Y)$$

Algorithm 4 INVERSE PROBLEM WITH CONTINUOUS SOURCE PARAMETER SPACE

PRECOMPUTE $\mathsf{U}^{\infty} \in \mathbb{R}^{N\times \mathrm{r}}$ IN $\mathcal{H}$-MATRIX FORMAT
for $\mathrm{i} = 1, \ldots, \mathrm{s}$ **do**
  DETERMINE THE iTH ROW OF THE LEAD FIELD BASIS $\mathsf{B}_{\mathrm{eeg}}^{\infty}$, $\mathsf{B}_{\mathrm{meg}}^{\infty}$
  MULTIPLY THIS ROW BY U^{∞}, I.E., COMPUTE iTH ROW OF L
  STORE iTH ROW IN $\mathrm{L} \in \mathbb{R}^{\mathrm{s}\times \mathrm{r}}$
end for
USE L FOR INVERSE METHODS ON DISCRETE PARAMETER SPACE

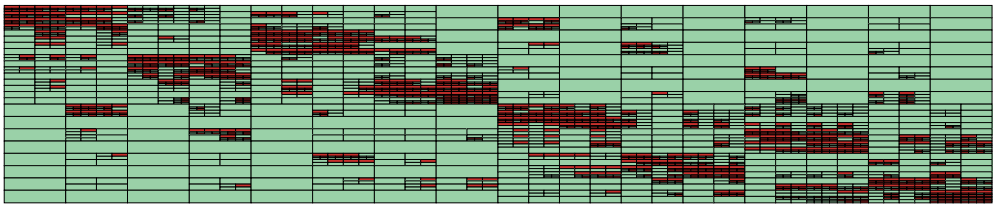

Figure 4. The transpose of the matrix U^∞ in $\mathcal{H}$-matrix format where each green block is stored in a data-sparse low-rank format.

for regions $X \times Y \ni (x, y)$ where we want to replace the function u^∞ by its interpolant (cf [50]).

Standard geometrically balanced clustering [49] yields a partition of the matrix U^∞ as shown in figure 4. Each green block in figure 4 allows for a data-sparse low rank approximation while the red (but small) ones are stored in standard dense matrix format. The whole matrix U^∞ can be assembled and stored with $c_{as} * \log(N) * N$ operations (81.4 s)—much less than the $c * \mathrm{r} * N$ operations (1026.8 s) needed without the data-sparse $\mathcal{H}$-matrix format. Once the matrix has been assembled and stored in this (packed) format, it allows for a fast matrix-vector multiplication with $c_{mv} * \log(N) * N$ operations (8.34 s) [49]. Algorithm 4 uses the $\mathcal{H}$-matrix format and exploits the fast matrix-vector multiplication. The total set-up complexity is

$$(i * k + c_{nz} + c_{mv} * \log(N)) * \mathrm{s} * N \qquad (5208.4\ \mathrm{s})$$

for the influence matrix L. This is 149 times less than the complexity for the state-of-the-art approach. The influence matrix L can, of course, be used for any inverse method working on that specific discrete influence space.

8. Conclusions and perspective

In this paper we presented a new approach to strongly reduce the algorithmic complexity of EEG/MEG inverse source reconstruction algorithms which are based on the finite element (FE) volume conductor modelling of the human head. The FE computational complexity of the state-of-the-art approach can be seen as the main disadvantage of FE compared to multi-layer sphere [10] or boundary element (BE) [11–13] head modelling. Our approach turns out to be very effective if the number of EEG/MEG sensors is much smaller than the number of sources for which a forward computation has to be carried out. This is the case in most applications, since the number of sensors is about 10^2, while the number of necessary forward computations is often beyond 10^4.

Our approach opens new possibilities concerning the resolution of FE head modelling. The number of large sparse linear systems that have to be solved per head geometry is now limited to the number of EEG/MEG sensors in order to compute the EEG/MEG lead field basis, a matrix with 'number of EEG/MEG sensors' rows and 'number of FE nodes' columns. The parallel algebraic multigrid preconditioned conjugate gradient method is an efficient solver for this set-up phase, as shown in [18, 20, 23, 26]. Each FE forward computation within inverse methods on both continuous and discrete source parameter space is then reduced to the multiplication of the FE right-hand side with the lead field basis. In combination with the blurred dipole model, a FE forward solution is then limited to $2 * \mathrm{s} * c_{nz}$ operations with s the number of EEG/MEG sensors and c_{nz} the number of neighbours to a FE node.

Furthermore, for the blurred dipole model [4, 18], we presented an algorithm for the row-wise computation of the influence matrix which only uses one row of the lead field basis

at a time so that the full lead field basis does not have to be stored at all. This method is suitable for all inverse methods on discrete source parameter space with high resolutions of the FE approach and a large number of EEG/MEG sensors.

The treatment of the mathematical dipole in the subtraction method [14, 18, 43] with our new approach is enhanced by using the data-sparse $\mathcal{H}$-matrix format.

The potential resolution for FE head modelling is now less limited by the complexity of the FE forward computations, but rather by the memory necessary to save the structures for the AMG-CG approach and the lead field basis. For very high resolutions, a parallel FE solver approach [18, 23] and the parallelization of the lead field basis multiplication seems to be necessary in order to distribute the memory on the computational nodes.

The new approach encourages the use and further development of the SimBio[4] mesh generation tool VGRID [51]. The current version of VGRID generates high-resolution FE meshes which are especially refined at tissue boundaries. In the future, a follow-up mesher could be developed in order to refine the FE mesh in areas of diffuse anisotropy.

The methods presented in this paper even motivate the use of the current resolution of the MR machines as the FE mesh resolution, i.e. FE meshing is no longer necessary at all.

Acknowledgment

The authors would like to thank Dr Alfred Anwander from the Max-Planck-Institute of Cognitive Neuroscience Leipzig for the discussions about reciprocity.

References

[1] Okada Y 1981 Neurogenesis of evoked magnetic fields *Biomagnetism* ed S N Erné, H D Hahlbohm and H Lübbig (Berlin: de Gruyter) pp 399–408

[2] de Munck J C, van Dijk B W and Spekreijse H 1988 Mathematical dipoles are adequate to describe realistic generators of human brain activity *IEEE Trans. Biomed. Eng.* **35** 960–6

[3] Nunez P L 1990 Localization of brain activity with electroencephalography *Advances in Neurology, Magnetoencephalography* vol 54 ed S Sato (New York: Raven Press) pp 39–65

[4] Buchner H, Knoll G, Fuchs M, Rienäcker A, Beckmann R, Wagner M, Silny J and Pesch J 1997 Inverse localization of electric dipole current sources in finite element models of the human head *Electroencephalogr. Clin. Neurophysiol.* **102** 267–78

[5] Andrä W and Nowak H 1998 *Magnetism in Medicine—A Handbook* (Berlin: Wiley–VCH)

[6] Geddes L A and Baker L E 1967 The specific resistance of biological material. A compendium of data for the biomedical engineer and physiologist *Med. Biol. Eng.* **5** 271–93

[7] Nicholson P W 1965 Specific impedance of cerebral white matter *Exp. Neurol.* **13** 386–401

[8] Rush S and Driscoll D A 1968 Current distribution in the brain from surface electrodes *Anesth. Analg.* **47** 717–23

[9] Akhtari M, Bryant H C, Marmelak A N, Heller L, Shih J J, Mandelkern M, Matlachov A, Ranken D M, Best E D and Sutherling W W 2000 Conductivities of three-layer human skull *Brain Topgr.* **13** 29–42

[10] de Munck J C 1988 The potential distribution in a layered anisotropic spheroidal volume conductor *J. Appl. Phys.* **64** 465–9

[11] Knösche T R 1997 Solutions of the neuroelectromagnetic inverse problem *PhD Thesis* University of Twente

[12] Fuchs M, Wagner M, Köhler T and Wischmann H A 1999 Linear and nonlinear current density reconstructions *J. Clin. Neurophysiol.* **16** 267–95

[13] Yvert B, Crouzeix-Cheylus A and Pernier J 2001 Fast realistic modeling in bioelectromagnetism using lead-field interpolation *Hum. Brain Mapp.* **14** 48–63

[14] Awada K A, Jackson D R, Williams J T, Wilton D R, Baumann S B and Papanicolaou A C 1997 Computational aspects of finite element modeling in EEG source localization *IEEE Trans. Biomed. Eng.* **44** 736–51

[4] SimBio: A generic environment for bio-numerical simulation. IST-programme of the European Commission, project no 10378, http://www.simbio.de, 2000–2003.

[15] Ollikainen J, Vauhkonen M, Karjalainen P A and Kaipio J P 1999 Effects of local skull inhomogeneities on EEG source estimation *Med. Eng. Phys.* **21** 143–54

[16] Weinstein D, Zhukov L and Johnson C 2000 Lead-field bases for electroencephalography source imaging *Ann. Biomed. Eng.* **28** 1059–66

[17] Haueisen J, Tuch D S, Ramon C, Schimpf P H, Wedeen V J, George J S and Belliveau J W 2002 The influence of brain tissue anisotropy on human EEG and MEG *NeuroImage* **15** 159–66

[18] Wolters C 2003 *Influence of Tissue Conductivity Inhomogeneity and Anisotropy on EEG/MEG-Based Source Localization in the Human Brain* (*MP Series in Cognitive Neuroscience* no 39) (Leipzig: MPI of Cognitive Neuroscience)
see also Wolters C 2003 *Dissertation* University of Leipzig, http://dol.uni-leipzig.de/pub/2003-33

[19] van den Broek S P, Reinders F, Donderwinkel M and Peters M J 1998 Volume conduction effects in EEG and MEG *Electroencephalogr. Clin. Neurophysiol.* **106** 522–34

[20] Wolters C H, Anwander A, Koch M, Reitzinger S, Kuhn M and Svensén M 2001 Influence of head tissue conductivity anisotropy on human EEG and MEG using fast high resolution finite element modeling, based on a parallel algebraic multigrid solver *Forschung und wissenschaftliches Rechnen* (*Contributions to the Heinz-Billing Award* no 58) (Göttingen Gesellschaft für wissenschaftliche Datenverarbeitung mbH) ed T Plesser, V Macho pp 111–157 See http://www. billingpreis.mpg.de

[21] Marin G, Guerin C, Baillet S, Garnero L and Meunier G 1998 Influence of skull anisotropy for the forward and inverse problem in EEG: simulation studies using the FEM on realistic head models *Hum. Brain Mapp.* **6** 250–69

[22] Anwander A, Wolters C H, Dümpelmann M and Knösche T R 2002 Influence of realistic skull and white matter anisotropy on the inverse problem in EEG/MEG-source localization *Proc. 13th Int. Conf. on Biomagnetism* ed H Nowak, J Hauiesen, F Giessler and R Huonker (Berlin: VDE) pp 679–81 http://biomag2002.uni_jena.de

[23] Wolters C H, Kuhn M, Anwander A and Reitzinger S 2002 A parallel algebraic multigrid solver for finite element method based source localization in the human brain *Comput. Vis. Sci.* **5** 165–77

[24] Reitzinger S 2001 Algebraic multigrid methods for large scale finite element equations *PhD Thesis* Schriften der Johannes-Kepler-Universität Linz, Reihe C-Technik und Naturwissenschaften no 36

[25] Haase G, Kuhn M and Reitzinger S 2002 Parallel AMG on distributed memory computers *SIAM J. Sci. Comput.* **24** 410–27

[26] Wolters C, Reitzinger S, Basermann A, Burkhardt S, Hartmann U, Kruggel F and Anwander A 2000 Improved tissue modeling and fast solver methods for high resolution FE -modeling in EEG/MEG-source localization. *Proc. 12th Int. Conf. on Biomagnetism (Helsinki 13–17 Aug)* ed J Nenonen, R J Ilmoniemi and T Katila pp 655–8 See http://biomag2000.hut.fi/papers_all.html

[27] Mohr M and Vamrunste B 2003 Comparing iterative solvers for linear systems associated with the finite difference discretisation of the forward problem in electro-encephalographic source analysis *Med. Biol. Eng. Comput.* **41** 75–84

[28] Helmholtz H L F 1853 Über einige Gesetze der Vertheilung elektrischer Ströme in körperlichen Leitern mit Anwendung auf die thierisch-elektrischen Versuche *Ann. Phys. Chem.* **89** 211–33, 354–77

[29] Malmivuo J and Plonsey R 1995 *Bioelectromagnetism: Principles and Applications of Bioelectric and Biomagnetic Fields* (New York: Oxford University Press)

[30] Vamrunste B, Van Hoey G, Van de Walle R, D'Havé M R P, Lemahieu I A and Boon P A J M 2001 The validation of the finite difference method and reciprocity for solving the inverse problem in EEG dipole source analysis *Brain Topogr.* **14** 83–92

[31] Nolte G 2003 The magnetic lead field theorem in the quasi-static approximation and its use for magnetoencephalography forward calculation in realistic volume conductors *Phys. Med. Biol.* **48** 3637–52

[32] Hämäläinen M S and Ilmoniemi R J 1984 Interpreting measured magnetic fields of the brain: estimates of current distributions *Technical Report* TKK-F-A559 Helsinki University of Technology

[33] Louis A and Maaß P 1990 A mollifier method for linear operator equations of the first kind *Inverse Problems* **6** 427–40

[34] Mosher J C, Lewis P S and Leahy R M 1992 Multiple dipole modeling and localization from spatio-temporal MEG data *IEEE Trans. Biomed. Eng.* **39** 541–57

[35] Wolters C H, Beckmann R F, Rienäcker A and Buchner H 1999 Comparing regularized and non-regularized nonlinear dipole fit methods: a study in a simulated sulcus structure *Brain Topogr.* **12** 3–18

[36] Schmitt U and Louis A K 2002 Efficient algorithms for the regularization of dynamic inverse problems: I. Theory *Inverse Problems* **18** 645–58

[37] Schmitt U, Louis A K, Wolters C H and Vauhkonen M 2002 Efficient algorithms for the regularization of dynamic inverse problems: II. Applications *Inverse Problems* **18** 659–76

[38] Scherg M and von Cramon D 1985 Two bilateral sources of the late AEP as identified by a spatio-temporal dipole model *Electroencephalogr. Clin. Neurophysiol* **62** 32–44
[39] Plonsey R and Heppner D 1967 Considerations on quasi-stationarity in electro-physiological systems *Bull. Math. Biophys.* **29** 657–64
[40] Nolting W 1992 *Grundkurs: Theoretische Physik, Elektrodynamik* (Ulmen: Zimmermann-Neufang)
[41] Sarvas J 1987 Basic mathematical and electromagnetic concepts of the biomagnetic inverse problem *Phys. Med. Biol.* **32** 11–22
[42] Pohlmeier R 1996 Lokalisation elektrischer Gehirnaktivität durch inverse Analyse des Magnetoenzephalogramms (MEG) mit Finite-Elemente-Modellen des Kopfes *Diplomarbeit in Elektrotechnik* RWTH Aachen
[43] von Rango J, Schlitt H A, Halling H and Müller-Gärtner H-W 1997 Finite integration techniques for the MEG forward problem *Quantitative and Topological EEG and MEG Analysis* ed H Witte, U Zwiener, B Schack and A Doering (Jena: Druckhaus Mayer) pp 336–8
[44] Lorente de No R 1938 Cerebral cortex: architecture, intracortical connections, motor projections *Physiology of the Nervous System* ed J F Fulton (Oxford: Oxford University Press) chapter 15
[45] Hackbusch W 1994 *Iterative Solution of Large Sparse Systems* (New York: Springer)
[46] Saad Y 1996 *Iterative Methods for Sparse Linear Systems* (New York: PWS Publishing)
[47] Börm S, Grasedyck L and Hackbusch W 2003 Introduction to hierarchical matrices with applications *Eng. Anal. Bound. Elem.* **27** 405–22
[48] Hackbusch W 1999 A sparse matrix arithmetic based on $\mathcal{H}$-matrices: I. Introduction to $\mathcal{H}$-matrices *Computing* **62** 89–108
[49] Grasedyck L and Hackbusch W 2003 Construction and arithmetics of $\mathcal{H}$-matrices *Computing* **70** 295–334
[50] Börm S and Grasedyck L 2002 Low-rank approximation of integral operators by interpolation *Technical Report* 72 Max Planck Institute for Mathematics in the Sciences (*Computing* at press)
[51] Basermann A, Berti G, Fingberg J and Hartmann U 2002 Head-mechanical simulations with SimBio *NEC Res. Devel.* **43**